

Cluster model for lattice distortion effects on electronic structure: VO and VO₂[†]

Michèle Gupta*

Department of Physics, Northwestern University, Evanston, Illinois 60201

D. E. Ellis

Departments of Physics and Chemistry, Northwestern University, Evanston, Illinois 60201

(Received 29 October 1975)

Molecular cluster predictions for electronic energy levels, wave functions, momentum densities, and Compton profiles of VO and VO₂ are examined within the Hartree-Fock-Slater model. VO₆ clusters are treated in O_h, D_{4h}, and D_{2h} symmetry to obtain quantitative relations between distortion parameters and level shifts and splittings. Effects of the crystal environment are taken into account by a potential field. Our results for VO are consistent with the augmented plane-wave band calculation of Mattheiss and x-ray emission data; the VO₂ levels are in good agreement with x-ray photoelectron spectroscopy data. A sizable anisotropy is predicted for the Compton profile of VO and VO₂.

I. INTRODUCTION

The varied and bizarre electronic transport and magnetic properties of transition-metal oxides are well known.¹⁻⁴ Despite considerable experimental and theoretical efforts, many aspects of the abrupt changes of electronic properties accompanying phase transitions in these materials are not understood. The roles of one-electron properties, *d*-electron localization, inter- and intra-atomic correlations, and defect and impurity structures have not been clearly established.

In this paper we apply the one-electron Hartree-Fock-Slater (HFS) theory to VO and VO₂ in an attempt to relate the properties of these two materials. Using molecular cluster approximations to the crystal we make a quantitative study of effects on electronic structure of lattice distortion from the perfect O_h octahedral metal-site symmetry of VO to the D_{2h} symmetry of VO₂ in the high-temperature rutile phase.

In Sec. II we discuss the one-electron model and computational methods used in this study. Electronic structure, crystal field splittings, and effects of lattice distortion are presented in Sec. III. In addition to relating the level structure of VO to that of VO₂, we are able to predict the effects of uniaxial stress on the optical spectra of VO. Our results compare favorably with the augmented plane-wave (APW) calculations of Mattheiss on VO,⁵ and with x-ray emission data.⁶ The VO₂ levels are in good agreement with the recent x-ray photoelectron spectroscopy (XPS) data of Blaauw *et al.*⁷

We also present results for wave functions. Effects of the crystal environment were taken into account by embedding the cluster in realistic external potentials. One-electron energies, and cluster wave functions were obtained (in a Slater-orbital basis) making use of the discrete variation-

al method.⁸ While self-consistent solutions were not obtained, effects of varying the assumed crystal charge distribution were examined. Although the conventional picture of ionic bonding with a full oxygen-2*p* valence band is verified, we do find a significant metal-ligand covalency. The covalent mixing between O-2*p* and V-3*d* is seen to be somewhat larger in VO₂, compared to VO. The increased valence bandwidth observed is due in large part to this interaction.

In Sec. IV momentum densities ρ(\vec{P}) are obtained by Fourier transforming the cluster eigenfunctions. Contributions to ρ(\vec{P}) from the partially occupied V-3*d* levels, and from the valence band are presented and the anisotropy in both VO and VO₂ is estimated. The resulting sizable anisotropy predicted for inelastic x-ray scattering suggests that Compton profile measurements would provide valuable new data allowing a precise comparison with model theories.

II. ONE-ELECTRON MODEL AND COMPUTATIONAL METHOD

A. Hartree-Fock-Slater model

The model Hamiltonian based upon Slater's statistical exchange approximation to the Hartree-Fock one-electron Hamiltonian is now very well known.⁹ In Hartree atomic units, it may be written

$$h_{\sigma} = -\frac{1}{2}\nabla^2 + V_c(\vec{r}) + V_{x,\sigma}(\vec{r}). \quad (1)$$

Here V_c is the usual Coulomb potential,

$$V_c = -\sum_{\nu} \frac{Z_{\nu}}{|\vec{r} - \vec{R}_{\nu}|} + \int d^3r' \frac{\rho(\vec{r}')}{|\vec{r} - \vec{r}'|} \quad (2)$$

and $V_{x,\sigma}$ is the local exchange potential for an electron of spin $s_x = \sigma$;

$$V_{x,\sigma} = -3\alpha[(3/4\pi)\rho_{\sigma}(\vec{r})]^{1/3}. \quad (3)$$

In the general spin-polarized case one obtains different wave functions and energies for either spin,

$$(h_\sigma - \epsilon_{n,\sigma}) \psi_{n,\sigma}(\vec{r}) = 0 \quad (4)$$

and the corresponding density is

$$\rho_\sigma(\vec{r}) = \sum_n f_{n,\sigma} |\psi_{n,\sigma}|^2. \quad (5)$$

The $f_{n,\sigma}$ are occupation numbers $0 \leq f_{n,\sigma} \leq 1$ which can be determined by Fermi statistics, or some more elaborate scheme. In the present work, only spin restricted solutions of Eq. 4 are treated; thus $\rho_\uparrow = \rho_\downarrow = \frac{1}{2}\rho$. The Hartree-Fock-Slater (HFS) eigenvalues and eigenfunctions to the Schrödinger equation are thus determined by the charge density. The exchange scaling parameter α can be assigned different values $\frac{2}{3} \leq \alpha \leq 1$ depending upon the method of derivation,^{10,11} or it can be treated as an adjustable parameter.

Ideally one would prefer to have self-consistent solutions to Eq. 4, obtained by the usual iteration on the charge density. However, a consistent solution for a molecular cluster embedded in a solid is made difficult by the boundary conditions. Therefore, we have investigated the level structure and wave functions determined by several assumed charge densities. The resulting model potentials span the range from neutral atom to fully ionic configurations, and thus are expected to encompass the results of self-consistent calculations. We wish to emphasize that the Coulomb and exchange potentials are evaluated according to Eqs. (2) and (3), without recourse to the usual "muffin-tin" spherical averaging approximations, which can lead to errors of several eV in the valence-electron energies.

B. Computational methods

The wave functions ψ_n are approximated by an expansion in symmetry adapted linear combinations of Slater-type orbitals centered on every nuclear site,

$$\psi_n(\vec{r}) = \sum_j \varphi_j(\vec{r}) C_{jn}. \quad (6)$$

The symmetry orbitals can be expressed as

$$\varphi_j(\vec{r}) = \sum_{\nu m} W_{\nu m}^{jl} R_{nl}(r_\nu) Y_{lm}(\hat{r}_\nu). \quad (7)$$

$W_{\nu m}^{jl}$ are the symmetrization coefficients obtained from group theory; n , l , and m are the quantum numbers of the atomic orbitals at site ν ; r_ν is the distance from nucleus ν to point r . The familiar secular equation

$$(\underline{H} - \epsilon \underline{S}) \underline{C} = 0 \quad (8)$$

is obtained and solved by use of the discrete varia-

tional method (DVM).⁶ In this method one chooses a finite grid of sample points $\{\vec{r}_p\}$ and defines a matrix element $\langle f \rangle$ as a weighted sum over the sample grid,

$$\langle f \rangle = \sum_p w(\vec{r}_p) f(\vec{r}_p). \quad (9)$$

By forcing certain error moments to vanish,

$$\langle \varphi_i^* (h - \epsilon_n) \psi_n \rangle = 0, \quad (10)$$

one obtains Eq. 8. When the weights $w(\vec{r}_p)$ are chosen to form an integration grid, the DVM solutions converge to the Rayleigh-Ritz integral solutions as the number of points is increased. The main advantages of the DVM are: (i) No restrictions are placed on the type or complexity of basis functions. (ii) No restrictions are placed on the form of the Hamiltonian. (iii) Since only discrete sums are evaluated the "multicenter integral problem" is avoided. (iv) Preliminary calculations can be made economically with a small number of sample points.

The STO basis set used in these calculations on VO₆ clusters is given in Table I. The oxygen basis is the "marginal" basis of Bagus *et al.*¹²; the vanadium basis, of roughly double ζ quality, was extended to include 4s and 4p character on the vanadium site. Some experimentation was done with orbital exponents, but no systematic parameter optimization was undertaken.

Charge densities ρ were obtained by summing spherical atomic (ionic) charge densities of free atoms (ions), calculated by means of the Herman-Skillman self-consistent field program.¹³

$$\rho = \sum_\nu \rho_\nu(|\vec{r} - \vec{R}_\nu|). \quad (11)$$

Previous MO and energy-band calculations on systems like¹⁴ MgO and¹⁵ TiS₂ have led to the conclusion that occupied levels of such ionic crystals were not very sensitive to choice of atomic/ionic configuration. Potentials constructed from HF or

TABLE I. Slater-type-orbital basis used for VO₆ cluster calculations.

V		O ^a	
$n\bar{l}$	ζ	$n\bar{l}$	ζ
1s	22.78	1s	7.38
2s, 2p	19.54	2s	9.569
2s, 2p	9.37	2s	2.3
3s, 3p, 3d	5.4	2p	3.692
3p	3.0	2p	1.656
3s, 3d	2.0		
4s	1.7		
4s, 4p	1.4		

^a"Marginal set," from Ref. 12.

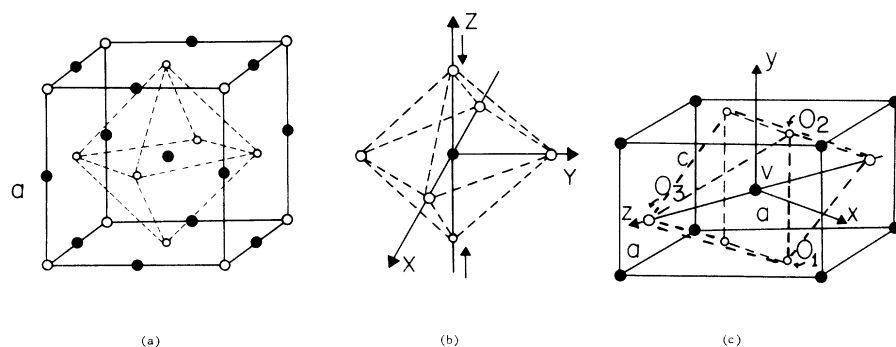


FIG. 1. Molecular clusters used in the calculation. Dark spheres are the vanadium atoms and open spheres the oxygen atoms. (a) Cubic unit cell of VO ($a = 7.735$ a.u.). Dashed lines indicate a VO_6 (O_h) cluster. (b) Distortion $O_h \rightarrow D_{4h}$ by compression along the z axis. (c) Tetragonal unit cell of rutile VO_2 ($a = 8.57947$ a.u., $c = 5.44249$ a.u.) $V-O_{(1)} = V-O_{(2)} = 3.606$ a.u., $V-O_{(3)} = 3.7006$ a.u. Dashed lines indicate a VO_6 (D_{2h}) cluster.

HFS atomic and ionic charge densities resulted in energy levels more or less rigidly shifted. Thus the APW calculations of Mattheiss⁵ on VO were based upon neutral atom HFS densities. However, our results show that the $O(2p) - V(3d)$ band gap is strongly affected by choice of potential, with neutral atom densities producing the most satisfactory picture.

III. ELECTRONIC STRUCTURE

A. Vanadium monoxide

VO has the rocksalt structure, with O_h octahedral point group symmetry about both metal and ligand sites [see Figs. 1(a)]. The bond length R_{V-O} is taken as 3.8675 a.u.,¹⁶ as indicated in Table II. (Lengths are given in Bohrs, and energies in Hartree a.u. unless specified otherwise.) While stoichiometric VO contains approximately 16% vacancies,¹⁷ theoretical models of the perfectly ordered crystal are of considerable interest. First-principles APW energy-band calculations have been reported by Mattheiss,⁵ and a linear combination of atomic orbitals (LCAO) band structure was obtained by Norwood and Fry.¹⁸ The semiempirical band model of Goodenough¹⁹ has been used to interpret optical and transport properties. Molecular cluster calculations using the semiempirical Mulliken-Wolfsberg-Helmholz method and the multiple scattering- $X\alpha$ (MS- $X\alpha$) method were performed by Gubanov *et al.*²⁰

Electrical conductivity measurements on VO_x , $0.8 < x < 1.3$, show semimetallic behavior for $x < 1.0$ and semiconducting properties for $x > 1$. The semiconductor energy gap is very small, $\sim 10^{-2} - 10^{-3}$ eV.²¹ Optical data do not seem to be available; however, x-ray emission data can be used to infer some features of the valence and conduction levels.⁶ High resolution XPS experiments would be similarly useful. X-ray data can be suc-

cessfully related to molecular orbital (MO) or cluster models for the solid; Fischer has given an empirical MO level scheme for a number of oxides, sulfides, etc.^{22,23}

We have previously shown for MgO ,¹⁴ and TiS_2 ,¹⁵ that the empirical MO model is supported and made quantitative by first-principles HFS cluster calculations. Work reported by Johnson *et al.* on NiO_6^{10-} complexes²⁴ and by Tossel *et al.* on anions²⁵ using the multiple-scattering technique (MS- $X\alpha$) further support the utility of cluster models. Of course, the results must be treated with care, since the desired external boundary conditions are not realized in practice. Thus the MS- $X\alpha$ method makes use of a surrounding charged sphere, and the DVM results depend upon the choice of external charge density. Furthermore, effects of the Pauli exclusion principle operating between cluster states and "exterior" states are generally ignored. With these reservations in mind we proceed to discuss our results on the octahedral VO_6 cluster, representative of crystalline VO.

It has been found that a superposition of *neutral*

TABLE II. Structural parameters for VO and VO_2 used in the present calculation.

	V-O distance along z axis ^a (in a.u.)	V-O distance in xy plane ^a (in a.u.)	$\theta = O-V-O$ angles in xy plane
VO^b	3.8675	3.8675	$90^\circ, 90^\circ$
VO_2^c	3.7006	3.6060	$82^\circ, 98^\circ$

^aAxes are indicated in Fig. 1.

^bFrom Ref. 16.

^cFrom Ref. 29. However, more recent determination of VO_2 lattice parameters by D. B. McWhan, M. Marezio, J. P. Remeika, and P. D. Dernier [Phys. Rev. B **10**, 490 (1974)] suggests a smaller lattice distortion for VO_2 .

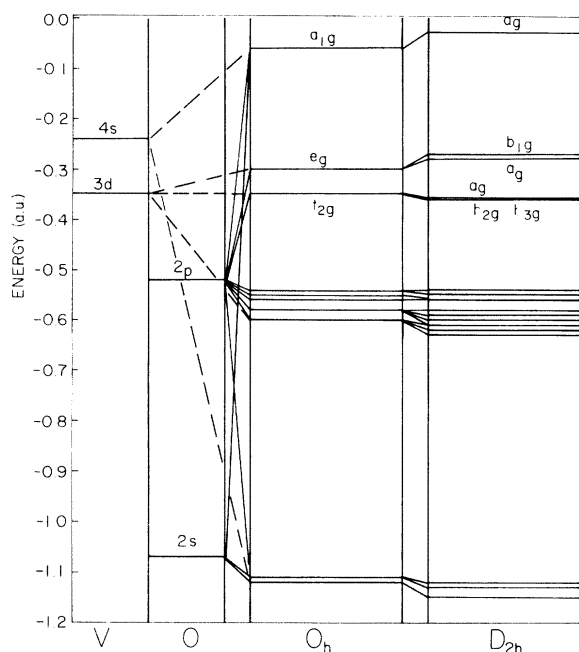


FIG. 2. Comparison of energy levels of free atoms, O_h cluster appropriate for VO crystal and D_{2h} cluster appropriate for VO_2 crystal, calculations were performed with the scaling exchange parameter $\alpha = 1.0$.

atom charge densities forms a good initial estimate of the crystal charge density, even for ionic systems.^{5,26} Therefore a series of *isolated cluster* calculations were carried out in this mode. Energy levels of VO_6 clusters with O_h and D_{2h} point group symmetries are shown in Fig. 2, along with the corresponding HFS atomic levels. About 2500 sample points were required by the DVM procedure in order to obtain a precision of ~ 0.1 eV in valence levels. The D_{2h} levels of VO_2 are discussed later; the O_h energy levels calculated with bond length $R_{V-O} = 3.8675$ a.u. appropriate for VO and with a value of the exchange scaling parameter of $\alpha = 1.0$ are presented in Table III.

TABLE III. Molecular energy eigenvalues for VO_6 cluster (O_g symmetry) in Hartree a.u.; the bond length R_{V-O} is that of the VO crystal. HFS neutral atom charge densities were used to construct the potential, with an exchange parameter $\alpha = 1$.

A_{1g}	E_g	T_{1g}	T_{1u}	T_{2g}	T_{2u}
-198.55	-19.77	-0.54	-19.77	-0.58	-0.56
-22.66	-1.11	+1.60 ^a	-19.33	-0.35 ^b	+1.48 ^a
-19.77	-0.60		-1.85	+0.73 ^a	
-2.78	-0.30 ^a		-1.11		
-1.12			-0.58		
-0.60			-0.55		
-0.06 ^a			+1.27 ^a		

^aUnoccupied.

^bHalf occupied.

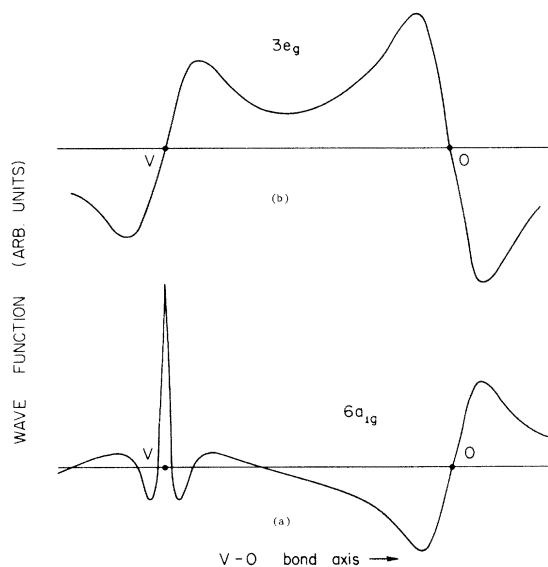


FIG. 3. VO_6 (O_h) valence eigenfunctions plotted along V-O bond direction (a) $6a_{1g}$ σ bonding $V_{3d}-O_{2p}$. (b) $3e_g$ σ bonding $V_{3d}-O_{2p}$.

Inner shell levels are not expected to be very accurate, because of the truncated basis and diffuse point sampling which was utilized.

The levels

$$(6a_{1g})^2 (3e_g)^4 (1t_{2g})^6 (1t_{2u})^6 (6t_{1u})^6 (1t_{1g})^6$$

form the "oxygen-2p" valence band. As predicted by the semiempirical description given by Goodenough¹⁹ the oxygen 2p band is separated from the next group of levels (principally of 3d-like character) by a large gap ~ 5.1 eV and hence will be fully occupied in the solid if we take into account the stoichiometry of the crystal. In the VO crystal, three electrons per vanadium atom remain to occupy the 3d levels. The width of the $O(2p)$ band from the $6a_{1g}$ level to the t_{1g} level is about 1.7 eV, comparable to the value of 1.9 eV given by Mattheiss's band calculation.⁵ In order to analyze the character of the wave functions, we plot as an example in Fig. 3, the wave functions for the $6a_{1g}$ and $3e_g$ levels, along one of the six equivalent V-O bonds. They show $V_{4s}-O_{2p}$ and $V_{3d}-O_{2p}$ bonding character, respectively. The strong mixture of metal d function with O_{2p} in the $3e_g$ valence level appears clearly in Fig. 3(b). The next level as we go up in the energy diagram is a π bonding $1t_{2g}$ state constructed from V_{3d} and O_{2p} functions while $1t_{1g}$ and $1t_{2u}$ are nonbonding ligand π states.

The half occupied $(2t_{2g})^3$ and unoccupied $4e_g$ levels, respectively, of π and σ antibonding $V_{3d}-O_{2p}$ character, have the ordering predicted by simple crystal-field theory. Thus the 3d orbitals of the metal lying between the ligands lead to more stable states than the 3d orbitals pointing towards

them; the level splitting is 1.4 eV. The fact that the $2t_{2g}$ level is half filled explains the observed metallic conductivity in the solid. This result is also in agreement with Mattheiss's band-structure calculation, where the Fermi level is found in the $3d$ band.⁵ The highest unoccupied level shown in Fig. 2, $7a_{1g}$, is an antibonding state of mainly V_{4s} character.

We see that the molecular cluster description leads to a charged cluster $(VO_6)^{10-}$ even when one starts from neutral atom densities. Self-consistent calculations for such anions require the imposition of an external stabilizing field. MS-X α calculations of this type have been performed by Gubanov *et al.*²⁷ However, one must carefully exclude "nonphysical" states occurring near the cluster bounding sphere.²⁷ We have made a number of calculations in which various modifications to the potential were explored. The results may be summarized as follows:

1. Effect of exchange scaling

All previously described results were obtained with the exchange scaling parameter $\alpha = 1.0$; decreasing α below 1.0 leads to less tightly bound levels. The differential shifts were such as to increase O($2p$)-V($3d$) band gap from 5.1 ($\alpha = 1.0$) to 6.5 eV for $\alpha = 0.7$. Other features were little changed. The value of the gap obtained with $\alpha = 0.7$ disagrees with x-ray emission data^{6,20} and hence all the results reported below will be calculated with $\alpha = 1.0$.

2. Effect of ionic potentials

Cluster potentials were generated corresponding to V^{2+} , O^{2-} free ion configurations, the latter having been calculated in a stabilizing potential well.²⁸ The main effect observed was an overall shift of levels toward less binding. Some significant changes in level ordering occurred, and relative shifts of ~ 5 eV were seen. For example the O($2p$)-V($3d$) gap (calculated with $\alpha = 1.0$) increased to 11.2 eV. By comparison with results for¹⁴ MgO one might expect that these ionic relative shifts are largely spurious, disappearing with the application of the external crystal potential. Unfortunately, the greater sensitivity of the V_{3d} level is apparent in these results, as discussed below.

3. Effect of external potentials

The octahedral VO_6 cluster was embedded in the potential field of the three nearest shells of neighbors. First, the charge density due to the superposition of neutral atoms was assumed, and the exchange parameter was taken as $\alpha = 1$. All occupied levels of the embedded cluster were lowered, compared to free-cluster results. Obviously levels constructed on oxygen functions, which

lie at the periphery of the cluster, are most strongly affected. As a consequence the O($2p$)-V($3d$) band gap is increased from 5.1 to 9.5 eV. This shift is certainly an overestimate, because of the neglect of Pauli exclusion between cluster and exterior.

Next, a potential corresponding to V^{2+} , O^{2-} ions was constructed for both the VO_6^{10-} cluster and the surrounding three nearest-neighbor shells. The effect of the external ionic potential was a decrease of the O($2p$)-V($3d$) band gap from 11.2 to 8.5 eV. Both values greatly exceed estimates from x-ray emission data.^{6,20} We conclude that the isolated cluster model, with potential generated from free atom densities is a good starting point, but that one would certainly prefer self-consistent embedded cluster results.

As pointed out previously, owing to the difficulty in obtaining good stoichiometric crystals, experimental data for VO are not as extensive as that for oxides of higher valency. In the absence of XPS data to provide energies of V and O inner levels in VO, we will follow the same absolute scale given by Gubanov *et al.*²⁰ The experimental spectra are reproduced from Ref. 20 in Fig. 4; the use of dipole selection rules gives a prediction of which molecular levels may participate in tran-

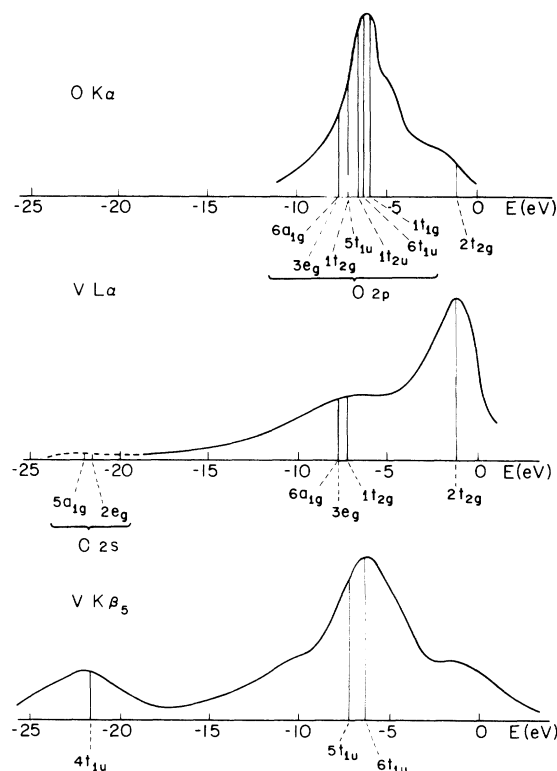


FIG. 4. Experimental x-ray emission spectra for VO from Ref. 20. Vertical lines indicate the position of the energy levels of VO_6 (O_h) cluster.

TABLE IV. Compatibility relations between representations of the point groups O_h , D_{4h} , and D_{2h} .

O_h	D_{4h}	D_{2h}
A_{1g}	A_{1g}	A_{1g}
E_g	$A_{1g} + B_{1g}$	$A_{1g} + B_{1g}$
T_{1g}	$A_{2g} + E_g$	$B_{1g} + B_{2g} + B_{3g}$
T_{1u}	$A_{2u} + E_u$	$B_{1u} + B_{2u} + B_{3u}$
T_{2g}	$B_{2g} + E_g$	$A_{1g} + B_{2g} + B_{3g}$
T_{2u}	$B_{2u} + E_u$	$A_u + B_{2u} + B_{3u}$

sitions to oxygen and vanadium core levels. The molecular cluster transitions are plotted against the experimental $O K\alpha$ ("1s - 2p"), $V L\alpha$ ("2p - 3d, 4s"), and $V K_{\beta 5}$ ("1s - 4p") spectra in the Fig. 4. To obtain an energy scale we matched the calculated O_{1s} level to the experimental O_{1s} energy obtained by Blaauw *et al.*⁷ by XPS data on a VO_2 crystal. The uncertainty caused by this procedure is expected to be of the same order of magnitude as that in aligning the experimental spectra.^{6,20} The calculated spectrum was thus shifted uniformly by 8.6 eV. As transition probabilities were not calculated, the height of the molecular lines shown in Fig. 4 is arbitrary. The calculated position of $O(2s)$, $O(2p)$, and $V(3d)$ bands is seen to be in good agreement with the x-ray emission data. The $O K\alpha$ spectrum suggests, however, that the gap $O(2p)$ - $V(3d)$ should be about 4 eV. Our "best" calculated value is 5.1 eV; a shift of this magnitude could certainly be expected from self-consistent core-relaxation effects. In addition, we may consider spin-polarization effects; MS- $X\alpha$ calculations²⁷ show that exchange splitting is small and reduces the $O(2p)$ - $V(3d)$ band gap by ~ 1 eV.

B. Distortions and level splittings

We have tested the response of the molecular cluster model to changes in the geometry, and the results obtained for the shifts and splittings of the molecular energy levels can be useful for describing the pressure dependence of the energy spectrum. Free-cluster calculations were made, starting from neutral-atom charge densities.

1. $O_h \rightarrow D_{4h}$ distortion

Starting with a VO_6 cluster corresponding to the geometry of the O_h point-group symmetry, we compressed the perfect octahedron by reducing the distance of the two vertical ligands on the z axis [see Fig. 1(b)]. This leads to the D_{4h} point-group symmetry. Of course the core levels of $1a_g \cdots 4e_u$ essentially retain their atomic character and are only slightly affected by symmetry changes. As the symmetry is lowered from O_h

to D_{4h} , the degeneracy of e_g and t_{1g} , t_{1u} , t_{2g} , and t_{2u} representations is respectively fully and partially lifted. The compatibility relations between representations of the point groups O_h and D_{4h} are listed in Table IV. Some valence levels remain unaffected by the compression of the octahedron along the z axis: they correspond either to non-bonding states constructed from orbitals of the planar ligands like $1b_{2u}$ and $1a_{2g}$ levels, or to bonding and antibonding states constructed from the planar ligands and vanadium functions having their lobes in the equatorial plane (like $3d_{xy}$ and $3d_{x^2-y^2}$); in the second category fall the bonding $3b_{1g}$, $1b_{2g}$, and antibonding $4b_{1g}$, $2b_{1g}$ states. But, as expected, a valence level like $5a_{2u}$ which corresponds to a σ bonding orbital (V_{pz} , O_{pz}) along the z axis becomes more stable as the V - O bond length on the z axis is decreased. The same trend is observed for all bonding levels involving the z -axis ligand: the $1e_g(V_{3d}, O_{p\pi})$ and $8a_{1g}(V_{3d}, V_{4s}, O_{pz})$ levels are lowered in energy.

For a relative compression of the octahedron by 10%, the stabilization of bonding levels increases the valence bandwidth by ~ 1 eV. Unfortunately, compressibility data do not seem to be available, so it is not possible to make a direct prediction of optical levels under axial stress.

In Fig. 5 we show the splittings $-\Delta E$ between several levels which are degenerate in O_h symmetry. Thus curves (a), (c), and (d) show the splittings of levels belonging to the O - $2p$ valence band, corresponding respectively to degenerate levels in " e_g ," " t_{2g} ," " t_{2u} " representations of the O_h point group. We note that levels of the valence band are very sensitive to the compression of the octahedron. The O_{2p} - V_{3d} gap increases at about a rate of 0.8 eV/a. u. with z -axis compression. We should point out that even though the metal-ligand interaction is described in terms of molec-

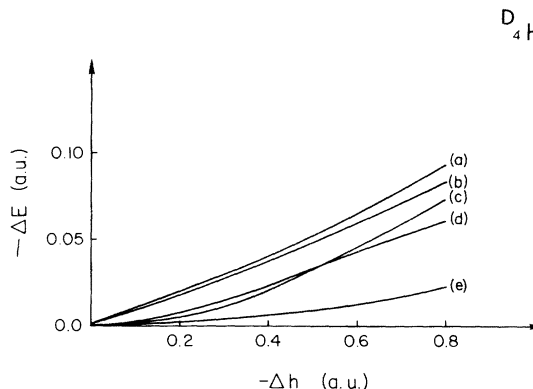


FIG. 5. Energy-level splittings owing to $O_h \rightarrow D_{4h}$ distortion; $-\Delta h$ is shift of axial ligand position in a. u. (compression). (a) $8a_g - 3b_{1g}$; (b) $4b_{1g} - 10a_g$; (c) $1e_g - 1b_{2g}$; (d) $6e_u - 1b_{2u}$; (e) $2b_{2g} - 3e_g$.

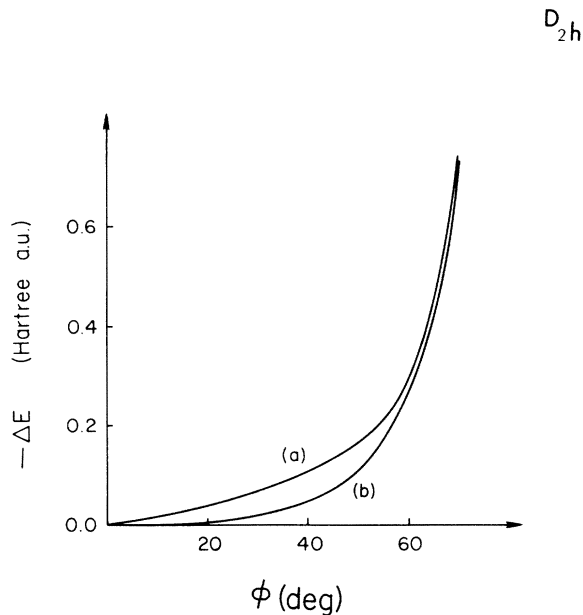


FIG. 6. Additional splittings owing to $D_{4h} \rightarrow D_{2h}$ distortion characterized by $\Phi = 90^\circ - \theta$, where $\theta = \text{O}_{(1)} - \text{V} - \text{O}_{(2)}$ angle. (a) $1b_{3g} - 1b_{2g}$; (b) $5b_{2u} - 5b_{3u}$.

ular orbitals in the cluster model, the splitting of the “ d ” levels, as the octahedral array of ligands becomes progressively distorted by reducing the distance of the two z -axis ligands, is in qualitative agreement with the predictions of simple crystal-field theory. Namely, the “ $d_{x^2-y^2}$ ” level ($4b_{1g}$) becomes more stable than “ d_{z^2} ” ($10a_g$) as shown in Fig. 5(b); the degenerate “ d_{xz} ,” “ d_{yz} ” ($3e_g$) levels become less stable than the “ d_{xy} ” ($2b_{2g}$) level [see Fig. 5(e)]. However, even for highly distorted configurations, the “ $d_{x^2-y^2}$ ” level does not drop below the degenerate “ d_{xz} ,” “ d_{yz} .” As could be expected, the departure from the perfect O_h symmetry is accompanied by a larger splitting of the e_g representation, than within the t_{2g} representation as it appears in Fig. 5 by comparison of curves (b) and (e). Some splittings are seen to be almost linear with compression; for example “ $d_{x^2-y^2} - d_{z^2}$ ” splitting (curve b) is ~ 2.5 eV/a. u.

2. $D_{4h} \rightarrow D_{2h}$ distortion

By a change in the value of $\theta(\text{O}_{(1)} - \text{V} - \text{O}_{(2)})$ angle in the $x-y$ plane, [see Fig. 1(c)] the symmetry is lowered from D_{4h} to D_{2h} . The degeneracy of the following representations: e_g , e_u of the D_{4h} point group is now lifted and the consequent splittings of the levels belonging to those representations are in some sense characteristic of the symmetry lowering. We show in Fig. 6 the splittings of occupied levels of the $\text{O}(2p)$ valence band as a function of $\Phi = 90^\circ - \theta$. The bond lengths of the octa-

dral array were taken from the values given by Westman,²⁹ characteristic of the rutile structure of metallic VO_2 . In Fig. 6(a) we show the ($1b_{3g} - 1b_{2g}$) splitting of π bonding combinations of ligand $2p$ functions and the $3d$ orbitals of vanadium. The π bond between planar ligand $2p_z$ and $\text{V} - d_{yz}$ becomes stronger as Φ increases, hence lowering the energy of the $1b_{3g}$ level. Since $1b_{2g}$ is constructed mainly on the $2p_x$ function of the vertical ligands and $3d_{xz}$ of the vanadium, it remains fairly constant. This metal-ligand interaction leads to a splittings of about 2 eV at $\Phi = 30^\circ$. The splitting observed in curve (b) is characteristic of the ligand-ligand interaction, marked by the formation of stronger bonds between the ligands in the xy plane, e.g., $5b_{2u}$ level. The level $5b_{3u}$, constructed mainly on the $2p_x$ functions of the vertical ligands, remains unaffected by the angular distortion. Nevertheless, let us mention that $5b_{2u}$ and $5b_{3u}$ levels have some residual V_{3p} character.

C. Vanadium dioxide

For temperatures above 340°K , VO_2 possesses the tetragonal rutile structure with the metal atom at a site of D_{2h} symmetry, see Fig. 1(c). The octahedral cluster considered for cubic VO can be distorted to the VO_2 geometry as follows (see also Table II): (i) A compression of the z -axis ligands to a distance $R_{\text{V-O}} = 3.7006$ a. u. (ii) A shear distortion in the $x-y$ plane which changes O-V-O angles from 90 to 82 and 98° , with bond distances $R_{\text{V-O}} = 3.606$ a. u. The low-temperature transformation to monoclinic structure is accompanied by a change in metal-metal distance and a semiconductor-to-metal transition.

The correlation diagram between the representations of O_h and D_{2h} point groups is given in Table IV, corresponding to the axes shown in Fig. 1. In lowering the symmetry of the octahedron from O_h to D_{2h} , the degeneracies of the molecular levels are fully lifted (see Table V). The oxygen valence band is spanned by the $8a_g \cdots 2b_{3g}$ levels, the bandwidth having increased from 1.7 (in VO) to 2.5 eV. The composition of the valence wave functions is quite similar to that found in O_h symmetry. The $8a_g$ state at the bottom of the band is a bonding combination of $2p$ functions on the planar ligands and the $3d_{x^2-y^2}$ function of vanadium. The top of the band is a nonbonding $\text{O}_{2p\pi}$ level with energy identical to that of the corresponding $1t_{1g}$ level in O_h symmetry, see Fig. 2. The valence levels corresponding to $\text{O}_{2p} - \text{V}_{3d}$ π bonding are less strongly bound than the corresponding σ bonding levels; however, they are more stable than predicted by Goodenough,¹⁹ and do not form a separate subband.

The value of the valence-to-conduction band gap (4.9 eV) is practically unchanged by the distortion of the octahedron. This value compares very

TABLE V. Molecular energy eigenvalues for VO_6 cluster (D_{2h} symmetry) in Hartree a.u.; the geometry is that of the VO_2 rutile structure. HFS neutral atom charge densities were used to construct the potential with an exchange parameter $\alpha = 1.0$.

A_g	B_{1g}	B_{2g}	B_{3g}
-198.55	-19.78	-0.60	-0.60
-22.66	-1.13	-0.55	-0.54
-19.78	-0.62	-0.36 ^a	-0.36 ^a
-19.77	-0.55	+0.75 ^b	+0.73 ^b
-2.79	-0.27 ^b		
-1.15	B_{1u}	B_{2u}	B_{3u}
-1.12	-19.77	-19.78	-19.78
-0.63	-19.34	-19.35	-19.33
-0.61	-1.85	-1.86	-1.86
-0.60	-1.12	-1.13	-1.12
-0.356 ^b	-0.59	-0.61	-0.58
-0.28 ^b	-0.56	-0.56	-0.56
-0.04 ^b	+1.25 ^b	-0.55	-0.56
	A_u	+1.26 ^b	+1.34 ^b
	-0.56		
	+1.54 ^b		

^aPartially occupied

^bUnoccupied

well with the energy gap of 4.5 eV at Γ found in the *ab initio* band-structure calculation of Mitra *et al.*,³⁰ starting with the potential of superimposed neutral atoms. We cannot compare our results with the band-structure calculation of Caruthers *et al.*,³¹ as these authors used a semiempirical potential chosen to give agreement with experimentally derived (optical) estimates of the $\text{O}(2p)$ - $\text{V}(3d)$ band gap of ~ 2.5 eV.

The " $t_{2g} - e_g$ " crystal-field splitting of the conduction band increases from 1.4 to 2.2 eV as we lower the symmetry from O_h to D_{2h} . The splitting of the t_{2g} level into $3b_{2g}$, $3b_{3g}$, and $11a_g$ is very small compared to the splitting of the e_g level. This is not surprising if we remember that the corresponding $d\pi$ orbitals lie between the ligands, and the geometry of the cluster of D_{2h} symmetry with an angle $\theta = 82^\circ$ in the xy plane is not very different from the D_{4h} point group ($\theta = 90^\circ$) for which the b_{2g} and b_{3g} representations are degenerate. The results obtained in our molecular cluster model lead to discrete molecular levels and cannot provide full information about the band width; however, the fact that $3d_{xz}$, $3d_{yz}$, and $3d_{x^2-y^2}$ form a group of quasidegenerate levels suggests that the corresponding bands in the solid will overlap. This is in agreement with the quali-

tative band picture given by Goodenough¹⁹ where the π antibonding d band is predicted to overlap with the so-called $d_{||}$ band. Of course, our model does not take into account the V-V interaction along the c axis; such an interaction could lower the $11a_g$ level. The results obtained by Sommers *et al.*,³² using the self-consistent MS- $X\alpha$ method to describe the cluster in D_{2h} symmetry also give three quasidegenerate $d\pi$ levels but with a somewhat different ordering. Since these authors only presented the d levels, we are unable to make detailed comparisons with our results.

Let us recall that in going from the O_h to the D_{2h} point group, the V-O bond lengths along the z axis are reduced by 4.5%, whereas the bond lengths in the xy plane are reduced by 7%. As the prism corresponding to the D_{2h} symmetry is longest in the z direction, we expect, as observed, the $12a_g(3d_{z^2})$ level to be more stable than the $5b_{1g}(3d)$ level constructed from orbitals pointing towards the ligands in the xy plane. These " e_g " levels are split by 0.3 eV. The small splitting of the d_π " t_{2g} " levels is consistent with a weak response to the variation of the angle, see Fig. 6.

The oxygen $2p$ "band" for the distorted cluster in VO_2 is found to be considerably lower in energy than the V ($3d$) band. Hence the O ($2p$) band will be filled in a VO_2 crystal and there remains only one $3d$ electron per vanadium atom in the $3b_{3g}$ level. This would correspond to a $(\text{VO}_6)^{8-}$ cluster.

In Fig. 7 we plotted our energy levels on the graph of the XPS spectrum given by Blaauw *et al.*,⁷ after matching the theoretical O_{1s} level to the experimental value given by these authors. To do

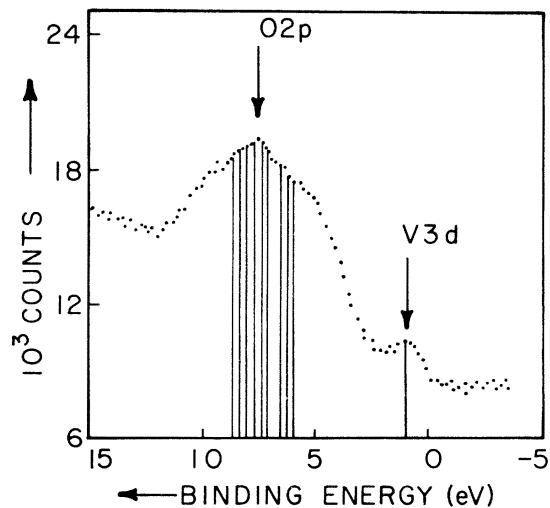


FIG. 7. Comparison with the experimental XPS data after Blaauw *et al.* (dotted curve) from Ref. 7. Vertical lines show the position of the energy levels of VO_6 (D_{2h}) cluster.

so we shifted our entire spectrum by 8.6 eV, as discussed previously. We then find the partially occupied $3d$ level to coincide with the peak "V_{3d}" observed experimentally. Similarly the group of levels forming the O ($2p$) band falls around the maximum of the broad experimental peak. The maximum of the peak coincides with a region of high density of states in our spectrum. Our calculation reproduces the essential features of the observed spectrum; we should, however, point out that this direct comparison of the one-electron energy spectrum to experimental values does not include the relaxation of the core orbitals during the photoemission process.

Verleur *et al.*³³ fitted optical reflectivity and transmission data for VO₂ to a classical oscillator model, obtaining two peaks in the imaginary part of the dielectric constant around 2.6 and 3.6 eV. This result was interpreted in a band model with the O ($2p$) band separated by a gap of ~ 2.5 eV from the partially occupied V ($3d$) band, in contrast to the value of 4.9 eV calculated here. The difficulties of obtaining a theoretical gap from *ab initio* calculations which would agree with these data has been discussed previously.³⁰ We made several further calculations to determine the dependence of this gap upon the form of the potential. An alternative atomic configuration for vanadium, $4s^1 3d^4$, was investigated, a reduction of the exchange scaling parameter from 1.0 to 0.7 was studied, and effects of the potential of external atoms (ions) were examined. In every case the band gap was increased over the 4.9 eV reported above.

IV. MOMENTUM DENSITIES AND COMPTON PROFILES

It has been known for many years³⁴ that broadening of the inelastic Compton x-ray line by the Doppler effect is related to the momentum distribution of electrons in the target. Experimental procedures and theoretical analysis have now progressed to a point where much useful information can be obtained about structure and bonding in solids^{35,36} by the inelastic scattering technique. While a rather large number of solids have been studied, there is a considerable need for the development of theoretical models capable of accurately describing the anisotropy and bonding effects which are observed. The molecular cluster approach offers attractive possibilities, providing that boundary-condition effects are not too serious.

Experimental Compton scattering data for the oxides seem to be limited to MgO,^{37,38} and NiO.³⁹ for MgO, Fukamachi and Hosoya⁴⁰ improved upon the O²⁻ "ion in a well" model by including solid-state effects obtained from Yamashita and Asano's spherically averaged Korringa-Kohn-Rostoker

(KKR) energy band charge density.⁴¹ However, the KKR wave functions were not directly used to calculate the Compton profile.

A. Momentum densities

Using the one-electron wave functions defined previously in Eq. (6), the momentum density can be written in the following way:

$$\rho(\vec{p}) = \sum_{i=1}^N n_i \chi_i^*(\vec{p}) \chi_i(\vec{p}), \quad (12)$$

where N is the total number of electrons, the n_i are the occupation numbers of the one-electron wave functions; $\chi_i(\vec{p})$, their Fourier transform in momentum space is

$$\chi_i(\vec{p}) = \frac{1}{(2\pi)^{3/2}} \int \psi_i(\vec{r}) e^{-i\vec{p}\cdot\vec{r}} d\vec{r}. \quad (13)$$

After expanding the plane wave in spherical harmonics and carrying out the angular integration one can show that

$$\chi_i(\vec{p}) = \left(\frac{2}{\pi}\right)^{1/2} (-i)^l \sum_j C_{ji} \sum_{\nu, m} W_{\nu m}^{jl} e^{-i\vec{p}\cdot\vec{R}_\nu} Y_{lm}^*(\hat{p}) Q_{nl}(p). \quad (14)$$

C_{ji} and $W_{\nu m}^{jl}$ are the linear combination coefficients defined in Eqs. (6), (7), \vec{R}_ν is the position vector of the ν th nucleus, $Q_{nl}(p)$ is the atomic integral defined in terms of the radial atomic function R_{nl} , and j_l is the Bessel function of order l :

$$Q_{nl}(p) = \int_0^\infty R_{nl}(t) j_l(pt) t^2 dt. \quad (15)$$

This integral was evaluated by using well-known analytic expressions.⁴² A study of the direction-dependent momentum density of the molecular clusters was made; our purpose here is to give an estimate of the anisotropies of the momentum density in VO and VO₂ crystals derived from the cluster model.

Obviously, the (VO₆)¹⁰⁻ cluster (appropriate for VO) and (VO₆)⁸⁻ results (appropriate for VO₂) cannot be used directly to represent crystal momentum densities. A simple scaling procedure was developed, by which the contributions of the oxygen valence and core levels were reduced to match the stoichiometry of the solid. Then it is possible to compare metal and ligand components of $\rho(\vec{p})$, and it is especially interesting to determine the magnitude and position of d -electron contributions. Figures 8–11 show the anisotropies of the momentum densities derived for VO and VO₂. For intermediate values of the momentum ($1 < p < 3$ a.u.) sizable anisotropies are observed. For example at $p = 2$ a.u. differences as large as 30% appear between the [100] and [110] directions for VO and between the [100] and [001] directions for VO₂.

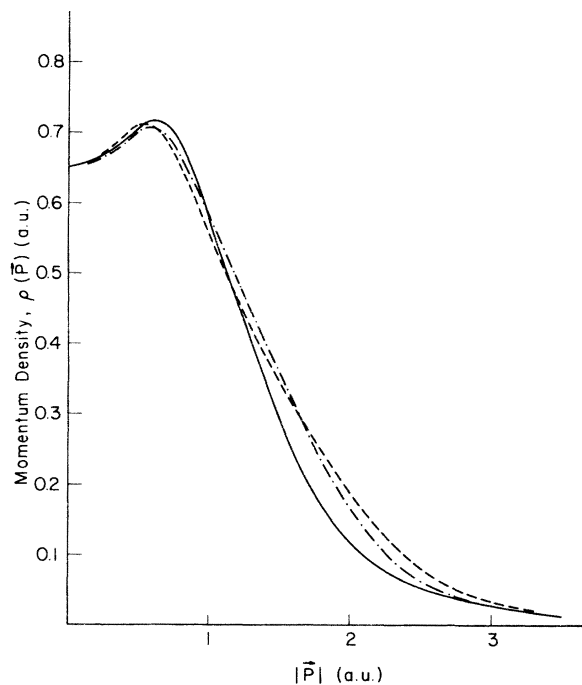


FIG. 8. Momentum density $\rho(\vec{P})$ for VO along several symmetry directions: (—) [100], (---) [110], (- · -) [111]; the total contribution.

For VO crystals, we note a decrease of the momentum density in the direction of the bond V-O relative to other directions. This general trend was also observed by Hennecker *et al.*⁴³ for diatomic molecules.

Let us recall that the value of $\rho(\vec{p})$ at $p=0$ is due to the contribution of the s -like functions; this con-

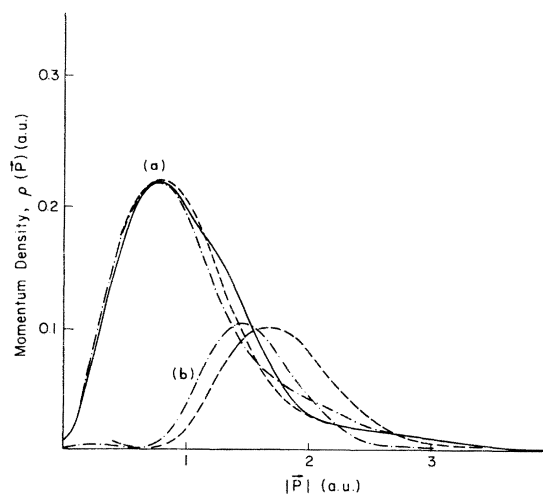


FIG. 9. Momentum density $\rho(\vec{P})$ for VO along several symmetry directions: (—) [100], (---) [110], (- · -) [111]. (a) Contribution from the O($2p$) band, and (b) "3d" electron contribution.

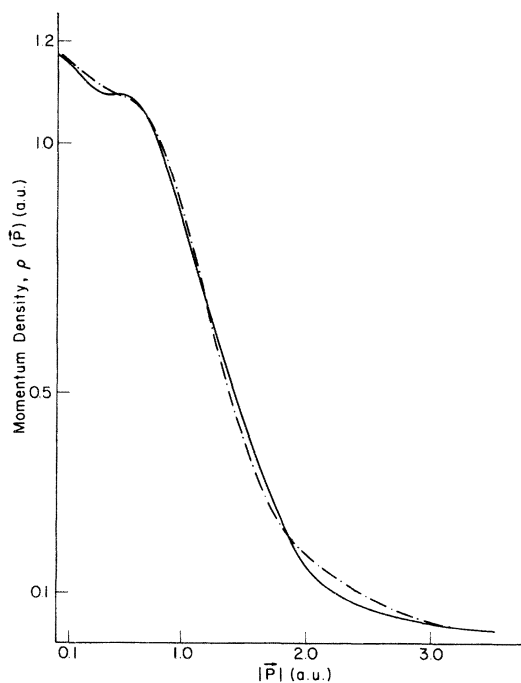


FIG. 10. Momentum density $\rho(\vec{P})$ for VO₂ along several symmetry directions: (—) [001], (---) [100]; the total contribution. N. B: Directions are relative to the axes shown in Fig. 1.

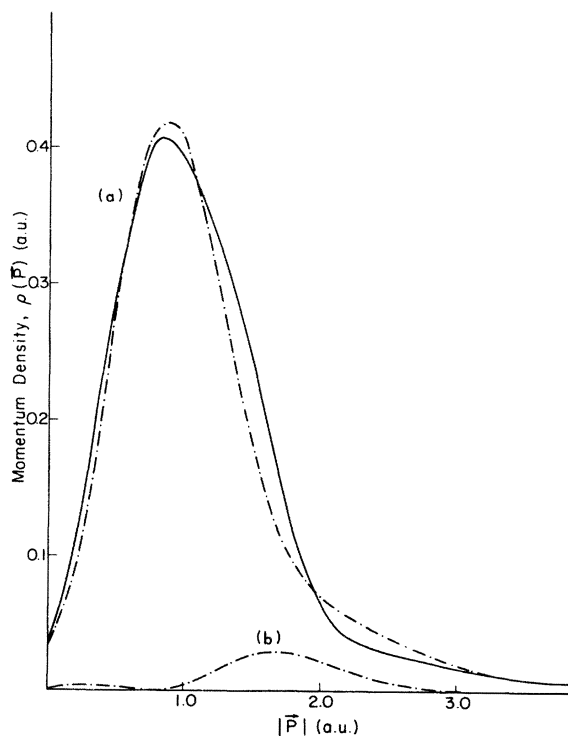


FIG. 11. Momentum density $\rho(\vec{P})$ for VO₂ along several symmetry directions: (—) [001], (---) [100]; (a) Contribution from the O($2p$) band; (b) "3d" electron contribution.

tribution decreases as p increases and is overwhelmed by the contribution of the valence electrons of the $O(2p)$ band, responsible for the structure observed around $p=0.6$ a.u.

The momentum density of the $O(2p)$ band and of the "3d" conduction electrons are plotted separately in curves (a) and (b) of Figs. 9 and 11. They allow us to understand the origin of the anisotropies in $\rho(\vec{p})$, which are seen to be mainly due to the conduction 3d electrons. Since the conduction levels are partially occupied, one may obtain varying degrees of anisotropy by populating the levels in different ways. We have chosen to display the *minimum* possible anisotropy, by filling the nearly degenerate " t_{2g} " levels uniformly (three electrons for VO, one electron for VO_2). For VO, for example, the contribution of the $3t_{2g}$ electrons reaches 0.1 for $1.5 < p < 1.8$ a.u. in [110] and [111] directions [which represents up to 30% of the total value of $\rho(\vec{p})$], while the contribution is zero in the [100] direction owing to symmetry considerations. However, sizable anisotropies of about 10% of the total value at $p=2\pi/a \approx 1.6$ a.u. appear in the momentum density of the $O(2p)$ valence band for both VO and VO_2 ; they are characterized by an increase of $\rho(\vec{p})$ along the direction of the bond, in the range of p values ($1.0 < p < 2.5$ a.u.) characteristic of the bonding. This result shows that even though the oxygen- $2p$ valence band is filled, the distribution in momentum space is far from spherical symmetry. The same remark can be made about the electron density in real space. The anisotropies in momentum space become negligible for large values of the momentum $p > 4$ a.u.

In order to estimate the bonding effect we compared the averaged probability density

$$I(p) = p^2 \int \rho(\vec{p}) d\vec{p} \quad (16)$$

of VO and of the superimposed free atoms in their ground state calculated with Clementi's⁴⁴ wave functions. We make this comparison with free atoms rather than ions, since the atomic charge densities proved to give more satisfactory potentials and energy levels. The function $I(p)$ is the probability of finding an electron with a momentum of given magnitude; the angular integration in Eq. (16) can be evaluated analytically in terms of vector-coupling coefficients. Figure 12 shows that the function $I(p)$ for VO and for the superimposed atoms coincide for large values of the momentum ($p > 5$ a.u.). As we expect, the contribution of the core electrons is not affected by the chemical bonding. The large difference for $p < 0.8$ a.u. arises mainly from the fact that the 4s electrons of the free $V(^4F)$ atom, responsible for this structure, are largely transferred to the ligands in VO. The differences observed for intermediate values of

the momentum, $1 < p < 3$ a.u., are more significant of the chemical bonding. The general trend observed in the formation of the cluster is a lowering of the probability function for small values of the momentum ($p < 1$ a.u.) and an increase of this function for intermediate values ($1 < p < 3$ a.u.), accompanying the formation of the bonds. This is in agreement with theoretical results obtained for molecules by several authors.⁴⁵⁻⁴⁷

B. Compton profile

If we use the impulse or "sudden" approximation which gives accurate results for weakly bound electrons and high incident photon energies,⁴⁸ the differential Compton scattering cross-section can be written

$$\begin{aligned} \frac{d^2\sigma}{d\omega d\Omega} &= \left(\frac{d\sigma}{d\Omega}\right)_{\text{Th}} \frac{\omega_1}{\omega_2} \int \rho(\vec{p}) \delta\left(\omega - \frac{k^2}{2m} - \frac{\vec{k} \cdot \vec{p}}{m}\right) d^3p \\ &= \left(\frac{d\sigma}{d\Omega}\right)_{\text{Th}} \frac{m\omega_1}{\omega_2} \frac{J(\vec{k}, q)}{|\vec{k}|}, \end{aligned} \quad (17)$$

where $(d\sigma/d\Omega)_{\text{Th}}$ is the Thompson cross-section per unit solid angle, $\hbar\omega$ is the energy transfer, $\omega = \omega_1 - \omega_2$, \vec{k} is the scattering vector $\vec{k} = \vec{k}_1 - \vec{k}_2$. The indices 1 and 2 refer to incoming and outgoing photons, respectively. In the inelastic collision,

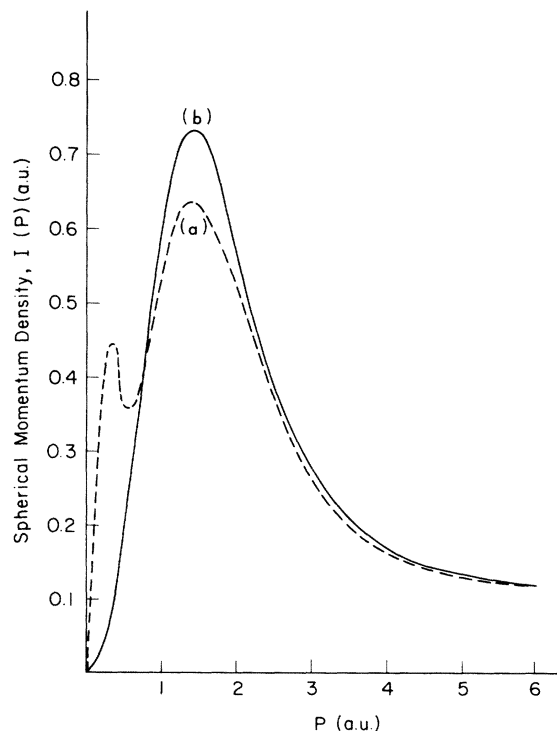


FIG. 12. Spherically averaged momentum density $I(P) = P^2 \varphi(P)/4\pi$ for (a) superimposition of the free atoms ($V+O$) calculated with Clementi's best functions from Ref. 44; (b) VO calculated with the cluster model.

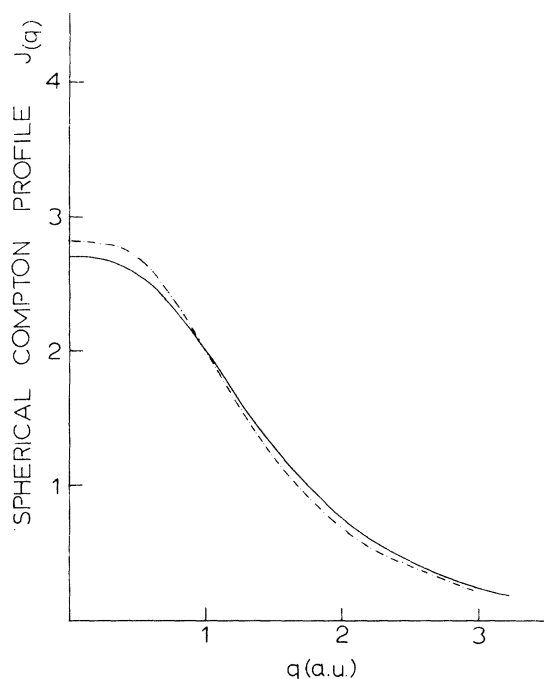


FIG. 13. Spherically averaged Compton profile of the valence and conduction electrons. Full line: VO; dot-dashed line: atomic model $V(3d^3 4s^0) + O(2p^6)$ constructed with Clementi's wave functions from Ref. 44.

energy conservation is expressed by means of the δ function. In the direction-dependent Compton profile $J(\hat{k}, q)$ the variable $q = \hat{k} \cdot \vec{p}$ is the projection of the electron momentum onto the unit scattering vector.

In Eq. (17) the presence of the δ function leads to an integration of the momentum density $\rho(\vec{p})$ in planes perpendicular to the scattering vector \hat{k} . In order to perform the integration and then obtain a direction-dependent Compton profile, we used a two-dimensional spline interpolation of the momentum density leading to about 98 000 interpolated points in each plane; our results are obtained with an accuracy of about 0.1%.

The spherically averaged Compton profiles defined as

$$J(q) = \frac{1}{2} \int_q^\infty \frac{I(p)}{p} dp \quad (18)$$

with the normalization condition $\int_{-\infty}^{+\infty} J(q) dq = N$ were also calculated. The one-dimensional integration in Eq. (18) was performed numerically, using Simpson's rule.

For Compton-profile calculations, unlike for momentum densities, we studied only the valence and conduction electrons; as pointed out previously, the impulse approximation cannot describe accurately the tightly bound core electrons of the vanadium atom. In Figs. 13 and 14, the spherically

averaged Compton profiles of the valence and conduction electrons for VO and VO₂ are compared to an atomic superposition model obtained by means of Clementi's⁴⁴ atomic functions. Realizing that the 4s electrons have been essentially transferred to the oxygen-2p band, we have occupied the atomic orbitals as $V(3d^3 4s^0)$, $O(2p^6)$; this model is in rough agreement (within 5%) with the cluster calculation. Comparison with a free-ion superposition model would not be very useful, since the O²⁻ density depends strongly upon the external boundary condition imposed.⁴⁰ As seen from the comparison of the averaged momentum densities, the molecular clusters show a greater extension of $I(p)$ in momentum space than the superimposed-atoms model does; therefore the value of the cluster Compton profile is expected to be smaller at $q=0$. The relative decrease $J(0)$ is of the order of 4% for both VO and VO₂. Consequently, if we keep in mind the normalization relation, the profile of the cluster is broader as observed in Figs. 13 and 14.

The contribution of the conduction electrons was plotted in Fig. 15 and compared with the atomic 3d averaged Compton profile obtained with Clementi's functions. $J(0)$ decreases by 10% from the free atom to the 3d electrons in VO. This general trend accompanying the formation of bonds has been

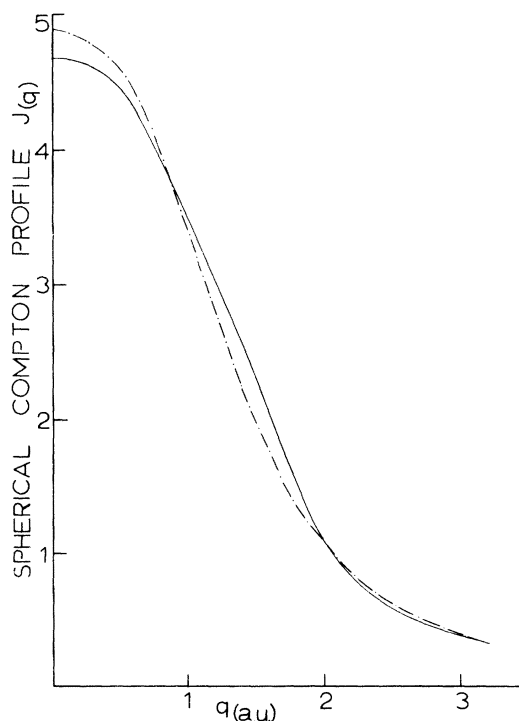


FIG. 14. Spherically averaged Compton profile of the valence and conduction electrons. Full line: VO₂; dot-dashed line: atomic model $V(3d^3 4s^0) + 2 \times O(2p^6)$ calculated with Clementi's wave functions from Ref. 44.

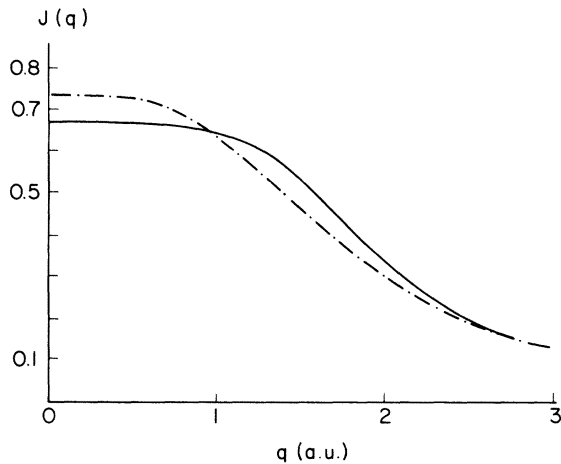


FIG. 15. Spherically averaged Compton profile: the separate contribution of the $3t_{2g}$ electrons in VO (full line) and the $3d^3$ electrons in the free V atom (dot-dashed line).

stressed by several authors.^{43,46,47} A comparison between the averaged Compton profile of one d electron in VO and VO_2 shows relative differences of the order of 1%, the Compton profile of the d electron in VO_2 being lower at $J=0$ and broader than in VO. This trend in momentum space can be associated in real space with a greater localization of the $3d$ electron in VO_2 than in VO. The anisotropies of the Compton profile appear in Figs. 16 and 17. For VO, the anisotropy between the [100] and [110] directions at $q=0$ represents about 3% of the total value and a maximum of 6% at $p=1.5$ a.u. For VO_2 the directions [001] and [100] show differences of the order of 1% of the total value at $q=0$; this reduction is primarily owing to the

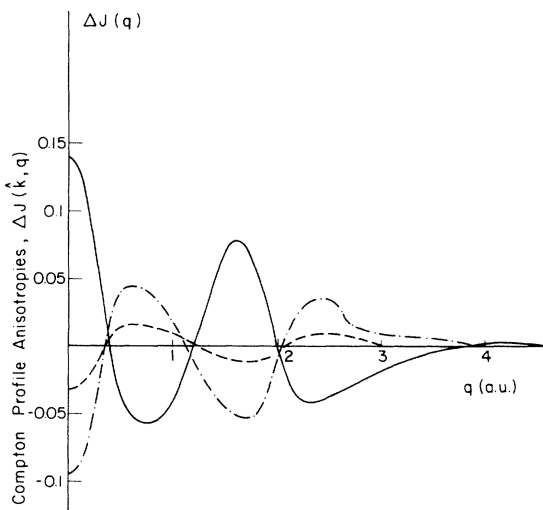


FIG. 16. Anisotropies of the Compton profile of VO for some directions; (—) $\Delta J = J_{\text{av}} - J_{100}$; (---) $\Delta J = J_{\text{av}} - J_{110}$; (- · -) $\Delta J = J_{2v} - J_{111}$.

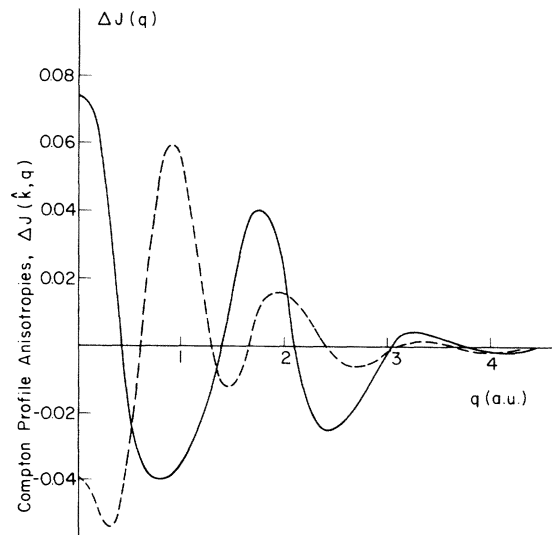


FIG. 17. Anisotropies of the Compton profile of VO_2 for some symmetry directions; (—) $\Delta J = J_{\text{av}} - J_{001}$; (---) $\Delta J = J_{\text{av}} - J_{100}$.

smaller number of d electrons in VO_2 . For both compounds, the Compton line shape along the direction of the V-O bond is broader, and has a lower value $J(0)$ than the Compton profile along a direction off the V-O bond. The same general trend has been observed experimentally on NiO samples³⁹; we hope that data on vanadium oxides will soon be available for comparison with our theoretical model.

C. Conclusion

We have seen that in vanadium oxides, the anisotropies are mainly due to the $3d$ electrons. However, the oxygen $2p$ band also contributes to the anisotropy, because of the covalent mixing with the $3d$ functions. For MgO, the experimental data show no significant anisotropy, since this compound is highly ionic with a full oxygen $2p$ band and no “ $3d$ ” electrons. Thus, Compton-profile measurements are an interesting probe for $3d$ electrons in transition-metal compounds. We have obtained differences of several per cent between direction-dependent Compton profiles, and a difference of the order of 1% between the spherically averaged Compton profiles for “ $3d$ ” electrons in VO and VO_2 . We may further speculate that a Compton-profile analysis could give measurable differences between the low- and high-temperature phases of the dioxide, where substantial bond length changes are observed.

ACKNOWLEDGMENT

The authors wish to thank Professor A. J. Freeman, A. Seth, E. Byrom, and V. A. Gubanov for helpful discussions during the course of the present work.

- †Research supported by the NSF through the Northwestern University Materials Research Center, and by the AFOSR, Grant No. 71-7012.
- ‡On leave from Le Centre de Mécanique Ondulatoire Appliqué du CNRS, 23, Rue du Maroc, 75019 Paris.
- ¹D. Adler, in *Solid State Physics*, edited by F. Seitz, D. Turnbull, and H. Ehrenreich (Academic, New York, 1968), Vol. 21 p. 1 and references therein.
- ²J. B. Goodenough, in *Progress in Solid State Chemistry*, edited by H. Reiss (Pergamon, Oxford, 1971), Vol. 5 p. 145.
- ³J. M. Honig, in *Fast Ionic Transport in Solids*, edited by W. Van Gool (North-Holland, Amsterdam, 1973), p. 311.
- ⁴R. N. Vest and J. M. Honig, in *Electrical Conductivity in Ceramics and Glass*, edited by N. M. Tallan (Marcel Dekker, New York, 1974).
- ⁵L. F. Mattheiss, Phys. Rev. B 5, 290; B 5, 306 (1972).
- ⁶V. M. Cherkashenko, E. Z. Kurmaev, A. A. Fotiev, and B. L. Volkov, Fiz. Tverd. Tela (to be published).
- ⁷C. Blaauw, F. Lennhouts, F. Van der Woude, and G. A. Sawatzky, J. Phys. C 8, 459 (1975).
- ⁸D. E. Ellis and G. S. Painter, Phys. Rev. B 2, 2887 (1970); T. Parameswaran and D. E. Ellis, J. Chem. Phys. 58, 2088 (1973).
- ⁹J. C. Slater, *The Self-Consistent Field for Molecules and Solids: Quantum Theory of Molecules and Solids* (McGraw-Hill, New York, 1974), Vol. 4, Chap. 1.
- ¹⁰J. C. Slater, Phys. Rev. 81, 385 (1951).
- ¹¹W. Kohn and L. J. Sham, Phys. Rev. 140, A1133 (1965).
- ¹²P. S. Bagus, T. L. Gilbert, and C. C. J. Roothaan, in Hartree-Fock Wave Functions of Nominal Accuracy for He through Rb⁺ Calculated by the Expansion Method (Argonne Nat. Lab. Interdivisional Studies in Chem. Phys. Argonne, Ill., 1972) (unpublished).
- ¹³F. Herman and S. Skillman, in *Atomic Structure Calculations* (Prentice-Hall, Englewood Cliffs, N.J., 1963).
- ¹⁴P. F. Walch and D. E. Ellis, Phys. Rev. B 8, 5920 (1973).
- ¹⁵D. E. Ellis and A. Seth, Int. J. Quantum Chem. 7, 223 (1973).
- ¹⁶W. B. Pearson, *A Handbook of Lattice Spacings and Structures of Metals and Alloys*, (Pergamon, New York, 1958).
- ¹⁷M. D. Banus and T. B. Reed, in *The Chemistry of Extended Defects*, edited by L. Eyring and M. O'Keefe (North-Holland, Amsterdam, 1970), p. 488.
- ¹⁸T. E. Norwood and J. L. Fry, Phys. Rev. B 2, 472 (1970).
- ¹⁹J. B. Goodenough, Bull. Soc. Chim. Fr. 4, 1200 (1965).
- ²⁰V. A. Gubanov, N. I. Lazukova, and E. Z. Kurmaev, Fiz. Mat. Met. Koord. Khim. Fiz. Dokl. Vses. Sovesch. 6-8, 64 (1974).
- ²¹J. B. Goodenough in *Annual Reviews in Materials Science.*, edited by R. A. Huggins, R. H. Bube, and P. W. Roberts (Annual Reviews, Palo Alto, Calif. 1971), Vol. 1, p. 101.
- ²²D. W. Fisher, in *Band Structure Spectroscopy of Metals and Alloys*, edited by D. Fabian and L. Watson (Academic, New York, 1973).
- ²³D. W. Fisher, App. Spectrosc. 25, 263 (1971).
- ²⁴K. H. Johnson, R. P. Messmer, and J. W. D. Connolly, Solid State Commun. 12, 313 (1973).
- ²⁵J. A. Tossel, D. J. Vaughan, and K. H. Johnson, Am. Mineral. 59, 319 (1974). For a survey of the work done by the MS-X α method, see K. H. Johnson, in *Computational Methods for Large Molecules and Localized States in Solids*, edited by F. Herman, A. D. McLean, and R. K. Nesbet (Plenum, New York, 1973).
- ²⁶J. C. Slater, *Quantum Theory of Molecules and Solids*, (McGraw-Hill, New York, 1965), Vol. 2.
- ²⁷V. A. Gubanov, J. Weber, and J. W. D. Connolly, J. Phys. Chem. Sol. 36, 861 (1975); and V. A. Gubanov (private communication).
- ²⁸R. E. Watson, Phys. Rev. 111, 1108 (1958).
- ²⁹S. Westman, Acta Chem. Scand. 15, 217 (1961).
- ³⁰T. K. Mitra, S. Chatterjee, and G. J. Hyland, Can. J. Phys. 51, 352 (1973).
- ³¹E. Caruthers, L. Kleinman, and H. I. Zhang, Phys. Rev. B 7, 3753 (1973).
- ³²C. Sommers, R. de Groot, D. Kaplan, and A. Zylbersztejn, J. Phys. Lett. 36, L157 (1975).
- ³³H. W. Verleur, A. S. Barker, Jr., and C. N. Berglund, Phys. Rev. 172, 788 (1968).
- ³⁴J. W. M. Du Mond, Rev. Mod. Phys. 5, 1 (1933).
- ³⁵R. J. Weiss, *X-ray Determination of Electron Distributions* (Wiley, New York, 1966).
- ³⁶M. Cooper, Adv. Phys. 20, 453 (1971), and references therein.
- ³⁷R. J. Weiss, Philos. Mag. 21, 1169 (1970).
- ³⁸S. Togawa, O. Inkinen, and S. Manninen, J. Phys. Soc. Jpn. 30, 1132 (1971).
- ³⁹T. Fukamachi, S. Hosoya, K. Iway, and K. Hayakawa, Phys. Lett. A 42, 477 (1973).
- ⁴⁰T. Fukamachi and S. Hosoya, J. Phys. Soc. Jpn. 31, 980 (1971).
- ⁴¹J. Yamashita and S. Asano, J. Phys. Soc. Jpn. 28, 1143 (1970).
- ⁴²J. D. Lyons and R. K. Nesbet, J. Comput. Phys. 47, 1634 (1969).
- ⁴³W. H. Hennecker and P. E. Cade, Chem. Phys. Lett. 2, 575 (1968).
- ⁴⁴E. Clementi, IBM J. Res. Dev. Suppl. 9, 2 (1965).
- ⁴⁵C. A. Coulson and W. E. Duncanson, Proc. Cambridge Philos. Soc. 37, 67 (1941); 38, 100 (1941).
- ⁴⁶I. R. Epstein and W. N. Lipscomb, J. Chem. Phys. 53, 4418 (1970).
- ⁴⁷A. Seth and D. E. Ellis, Phys. Rev. A (to be published).
- ⁴⁸P. Eisenberger and P. M. Platzman, Phys. Rev. A 2, 415 (1970).